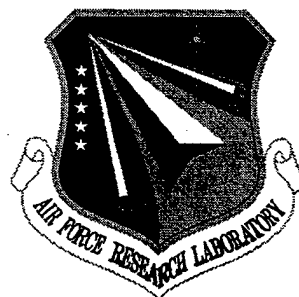AFRL-SN-RS-TR-1998-33
Final Technical Report
March 1998

PROPAGATION OF A GAUSSIAN-BEAM IN A BACTERIORHODOPSIN FILM

Syracuse University

Q. Wang Song

19980512 003

AIR FORCE RESEARCH LABORATORY
SENSORS DIRECTORATE
ROME RESEARCH SITE
ROME, NEW YORK

DTIC QUALITY INSPECTED 3

This report has been reviewed by the Air Force Research Laboratory, Information Directorate, Public Affairs Office (IFOIPA) and is releasable to the National Technical Information Service (NTIS). At NTIS it will be releasable to the general public, including foreign nations.
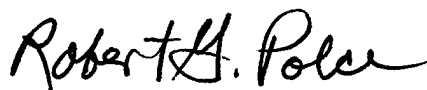
AFRL-SN-RS-TR-1998-33 has been reviewed and is approved for publication.

APPROVED: *John Malowicki*

JOHN E. MALOWICKI
Project Engineer

FOR THE DIRECTOR: *Robert G. Polce*

ROBERT G. POLCE, Acting Chief
Rome Operations Office
Sensors Directorate

If your address has changed or if you wish to be removed from the Air Force Research Laboratory Rome Research Site mailing list, or if the addressee is no longer employed by your organization, please notify AFRL/SNDP, 25 Electronic Pky, Rome, NY 13441-4515. This will assist us in maintaining a current mailing list.

Do not return copies of this report unless contractual obligations or notices on a specific document require that it be returned.

REPORT DOCUMENTATION PAGE

Public reporting burden for this collection of information is estimated to average 1 hour per response, including the time for reviewing instructions, searching existing data sources, gathering and maintaining the data needed, and completing and reviewing the collection of information. Send comments regarding this burden estimate or any other aspect of this collection of information, including suggestions for reducing this burden, to Washington Headquarters Services, Directorate for Information Operations and Reports, 1215 Jefferson Davis Highway, Suite 1204, Arlington, VA 22202-4302, and to the Office of Management and Budget, Paperwork Reduction Project (0704-0188), Washington, DC 20503.

1. AGENCY USE ONLY *(Leave blank)*	2. REPORT DATE	3. REPORT TYPE AND DATES COVERED
	April 1998	FINAL . Apr 96 – Oct 97

4. TITLE AND SUBTITLE
PROPAGATION OF A GAUSSIAN-BEAM IN A BACTERIORHODOPSIN FILM

5. FUNDING NUMBERS
C - F30602-96-C-0066
PE - 62702F
PR - 4600
TA - P5
WU - PL

6. AUTHOR(S)
Q. Wang Song

7. PERFORMING ORGANIZATION NAME(S) AND ADDRESS(ES)
Syracuse University
Office of Sponsored Programs
113 Bowne Hall
Syracuse NY 13244-1200

8. PERFORMING ORGANIZATION REPORT NUMBER

9. SPONSORING/MONITORING AGENCY NAME(S) AND ADDRESS(ES)
Air Force Research Laboratory/SNDP
25 Electronic Pkwy
Rome NY 13441-4515

10. SPONSORING/MONITORING AGENCY REPORT NUMBER

AFRL–SN–RS–TR–1998–33

11. SUPPLEMENTARY NOTES
Air Force Research Laboratory Project Engineer: John Malowicki, SNDR, (315) 330-4682

12a. DISTRIBUTION AVAILABILITY STATEMENT
APPROVED FOR PUBLIC RELEASE: DISTRIBUTION UNLIMITED

12b. DISTRIBUTION CODE

13. ABSTRACT *(Maximum 200 words)*

Presented is a computational study on the Gaussian-beam propagation in the bio-optical material bacteriorhodopsin with considerations of the material's intensity-dependent absorption and refractive index modulation. The beam focusing size, focusing position, intensity change in the material and their dependence on the incident beam parameters are simulated. Results of the simulation have application to the limits on memory storage in bacteriorhodopsin.

14. SUBJECT TERMS
bacteriorhodopsin, Gaussian-beam propagation, absorption, refractive index, intensity

15. NUMBER OF PAGES
36

16. PRICE CODE

17. SECURITY CLASSIFICATION OF REPORT	18. SECURITY CLASSIFICATION OF THIS PAGE	19. SECURITY CLASSIFICATION OF ABSTRACT	20. LIMITATION OF ABSTRACT
UNCLASSIFIED	UNCLASSIFIED	UNCLASSIFIED	UL

Table of Content

List of Figures

Abstract

This report presents the computational study on the Gaussian-beam propagation in the bio-optical material bacteriorhodopsin with considerations of the material's intensity-dependent absorption and refractive index modulation. The beam focusing size, focusing position, intensity change in the material and their dependence on the incident beam parameters are simulated.

I.   Introduction

Three-dimensional (3-D) optical memories [1-3] show great promise for data storage and retrieval because of its high capacity. It is regarded as a potential candidate for future high-performance digital applications, such as multimedia and video on demand, and military and industrial object recognition applications. Optical memory technology poses challenges for scientists to search for an ideal photoactive material. The photochromic protein bacteriorhodopsin (BR) [4] is a material that demonstrates real-time information recording capabilities and has a promising information-storage potential [5]. BR undergoes a complex photocycle on the absorption of light energy. The two relevant photochemical states are called bR and M states with bR being the ground and M being the thermal intermediate states, respectively. The bR state has a strong absorption in the green-yellow region of the visible spectrum (λ_{max} = 568 nm). The M state exhibits a strong blue-shifted absorption spectrum (λ_{max} = 412 nm). When a beam is traveling in this material, the absorption and phase modulation are both wavelength- and intensity-dependent. Further propagation of the beam is affected by these light-induced processes.

In both two-photon absorption [7,8] or Fourier transform hologram types of 3-D optical memories, the beam focusing property plays an essential role in determining the information storage density and addressing accuracy. To be specific, the storage density in BR or other storage materials depends on how small a light spot can be formed in the material. The smaller the spot, the higher the possible storage density. In addition, the

location of the focused light spot needs to be accurately determined for optimum distribution and precise addressing of stored data. Because of the nonlinear wavefront modulation of BR, the above issues become quite involved and depend on the wavelength, beam power and divergent angle, as well as the material properties.

In this report, we present the computational study on the steady state behavior of a Gaussian beam as it passes through a BR film. We find that the beam waist and its location in BR are all greatly changed due to the nonlinearity of BR. In addition, the maximum intensity no longer takes place at the beam waist. All these properties may be important when the material is used for volume Fourier transform holographic memory and/or two-photon absorption optical memory. The study of Gaussian beam propagation is useful for future studies on BR as an optical memory medium. This study can also be used as a reference to other absorption and index modulation recording materials, where the recording density is also ruled by the resolution the imaging system can achieve. In previous reports, [6,9] we have presented the experimental determination of the effective nonlinearity of BR film. The parameters for the absorption of the BR film were also reported. [10] Our simulations are based on these parameters.

II.   Optical properties of bacteriorhodopsin material

Bacteriorhodopsin is a light transducing protein found in the purple membrane of the organism *Halobacterium salinarium*. This bacterium grows in salt marshes, where the concentration of salt is six times that of seawater. A BR molecule pumps a proton across the

bacterium's membrane when it absorbs light, thus generates a chemical and osmotic potential that serves as an alternative source of energy.

The number of times that BR can be cycled photochemically – switched optically from one state to another – is about ten million times, a value considerably higher than that of most synthetic photochromic materials, which can cycle form 100 to 10,000. Therefore, the common perception that biological materials are too fragile for use in optical devices does not apply to BR.

The absorption of light energy by theretinyl chromophore initiates a complex photocycle characterized by several spectroscopically distinct thermal intermediates and a cycle time of 10 ms. The large shift in absorption maxima accompanying the BR to M phototransformation generates a corresponding linear change in the refractive index which is key to many optical processing applications.

BR has been reported to be suitable for three-dimensional (3-D) optical memories [8]. Two-photon absorption is regarded the one of the prime factors for the information recording in 3-D optical memories. The forward reaction from bR state to M state is driven by two 1,140-nm photons, and the reverse reaction from M state to bR state is driven by two 820-nm photons.

III. Concept of a 3-D optical memory
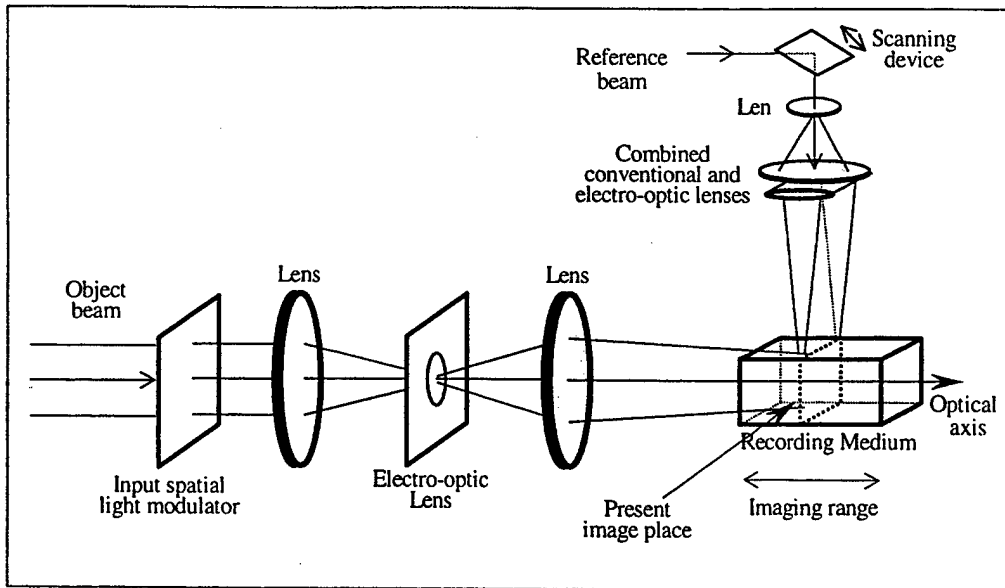
Figure 1. A 3-D optical memory information storage and retrieval.

Figure 1 shows a typical system for two-photon absorption 3-D optical memory. The object beam is used as the information carrier when it transmits through the transmission input spatial light modulator (SLM). The to-be-recorded information is electrically written on the SLM. The object is imaged onto the recording medium by a combination of lenses including a variable focus-length lens on the Fourier plane. The reference beam is the other arm of the system for the two-photon absorption photochromic recording of information. Reference beam is also controllable by a combined lens consisting of conventional lenses and an electro-optic lens. The reference beam may produce a sheet of light to cover the image plane of the SLM. Two-photon absorption occurs at the interaction section of the two beams. Thus the two-dimensional information is recorded at

4

once. When the variable focus-length lens adjusts its focal length, the image plane of SLM shifts along the optical axis in the recording medium. The light sheet traces the image plane through a scanning device. Thus information can be recorded in the medium page by page. The page information storage capacity in the media is limited by the thickness of the sheet-of-light.

Since there is a physical limitation, although the process is massive parallel, the sheet of light concept does permit a high recording density. It is impossible to produce a sheet of light with thin thickness. But it is easy to achieve a fine line of light. Thus as an alternative, we proposed the concept of scanning line-of-light. The information recording is performed line by line instead of page-by-page. Although parallelism is sacrificed compared with the later, the line-by-line recording still maintains a very high parallelism as compared with the current serial method by today's computer industry. And because the line-of-light can be very thin (only limited by the real system design), high recording density is surely promised.

Three-dimensional memory can also be implemented by using focusing point of light in both of reference and object beams. This will give a memory using serial recording and information retrieval. We can achieve the highest recording density but sacrifice operation time.

Three-dimensional memories are also reported with other techniques, such as wavelength and angular multiplexing. The storage space for wavelength and angular multiplexing are overlapped in the recording medium, thus suffering low recording and diffraction efficiencies. Whichever scheme is chosen for the 3-D optical memory

implementation, the laser beam's propagation is the essential. Thus a study of the properties of Gaussian beam propagation in the concerned recording medium is of great interest.

IV.   Modeling and Analysis

A Gaussian beam in a uniform linear medium is characterized by a Gaussian amplitude profile and a quadratic phase distribution, which is mathematically expressed as [11]

$$E(x, y; z) = E_0 \frac{W_0}{W(z)} \exp\left[-\frac{\rho^2}{W^2(z)}\right] \exp\left[ikz + ik\frac{\rho^2}{2R(z)} - i\phi(z)\right], \qquad (1)$$

where k is the wave number of the Gaussian beam in the medium, W_0 is the waist size, and E_0 is the field amplitude at the waist position,

$$W^2(z) = W_0^2\left(1 + \frac{z^2}{z_0^2}\right), \qquad (2)$$

$$z_0 = \frac{\pi W_0^2 n_0}{\lambda} = \frac{k W_0^2 n_0}{2}, \qquad (3)$$

$$R(z) = z\left[1 + \left(\frac{z_0}{z}\right)^2\right], \qquad (4)$$

$$\phi(z) = \tan^{-1}\left(\frac{z}{z_0}\right), \qquad (5)$$

n_0 is the intrinsic index of refraction of the medium. In a nonlinear medium, however, the amplitude, phase, and divergence angle will be modulated by the light field itself.

BR is a material that demonstrates saturable absorption and phase modulation properties. The intensity-dependent exponential absorption constant at the steady state can

6

be expressed by [10]

$$\alpha(I) = N\sigma_1 \left[\frac{1 + 2\sigma_2 \tau I / h\nu}{1 + (\sigma_1 + \sigma_2)\tau I / h\nu} \right] = \alpha_0 - \frac{gI}{1 + I/I_s}, \tag{6}$$

where $\alpha_0 = N\sigma_1$, $g = N\sigma_1(\sigma_1 - \sigma_2)\tau / h\nu$, $I_s = h\nu / (\sigma_1 + \sigma_2)\tau$ is the saturation intensity,

N is the active density of BR molecules, σ_1 and σ_2 are the absorption cross sections for the

nonradiative transitions $bR \Rightarrow M$ and $M \Rightarrow bR$, τ is the relaxation time for the transition

$M \Rightarrow bR$, ν is the frequency. The saturation intensity, I_s, depends on the lifetime of the M

state and the absorption cross-sections of the BR material. For the laser wavelength of 632.8

nm, the typical parameters for BR-doped polymer films in the above equation are [9,10]

$$\begin{aligned} \alpha_0 &= 8.2 \quad cm^{-1} \\ I_s &= 4.1 \quad mW/cm^2 \; . \\ g &= 0.83 \quad cm/mW \end{aligned} \tag{7}$$

For the laser wavelength of 514.5 nm, the typical parameters are [9,10]

$$\begin{aligned} \alpha_0 &= 17.2 \quad cm^{-1} \\ I_s &= 9.5 \quad mW/cm^2 \; . \\ g &= 1.23 \quad cm/mW \end{aligned} \tag{8}$$

For BR prepared with different options, the parameters may have values different from Eqs.

(7) and (8). The saturation intensity, for example, is a function of the lifetime of the M state,

which can be changed by chemical enhancement or other method [6]. However, the

simulations with these numbers yield typical BR behavior. The intensity-induced phase

change under low intensities can be expressed by [9,12]

$$n = n_0 + \Delta n(I) = n_0 + n_2 I, \tag{9}$$

where $n_0 = 1.5$, $n_2 = -1.25 \times 10^{-7}$ cm^2/mW for 632.8 nm wavelength and $n_2 = +1.25 \times 10^{-7}$

7

cm^2/mW for 514.5 nm wavelength. n_2 may have different values depending on the individual preparation process of the BR film [9]. Eq. (9) may be held correct when I is small. When it is getting larger, the index change will reach to nonlinear maximum until the thermal effect take place. [10] At that point we may assume a formula for the relationship between the index change and the intensity [9,14]

$$\Delta n(I) = \frac{n_2 I}{1 + \dfrac{I}{I_0}},$$

(10)

The maximum of Δn is assumed [13,14] to be -1.0×10^{-3} for red light and 1.0×10^{-3} for green light, respectively. Both n_2 and I_0 are functions of molar refraction coefficients and concentrations of the M and bR states. Therefore, with n_2 and the maximum Δn known, we have the estimation of I_0

$$I_0 = \frac{[\Delta n]_{max}}{n_2} = 8.0 \times 10^3 \ \text{mW/cm}^2.$$

(11)

The propagation of a coherent paraxial beam through a distance d in a uniform and linear medium can be obtained by using the spatial transfer function for propagation of d distance in that medium. We modify this method to study the light field evolution of a Gaussian beam during its propagation in the BR film. We treat the propagation in two steps: first, the nonlinear amplitude and phase modulation due to the BR material and second, the diffraction effect of wave propagation. We assume that the intensity distribution of the Gaussian beam in the input plane of a differential layer of thickness d determines the absorption and phase modulation properties of this layer. So the nonlinear wave modification by this layer can be modeled as an infinitely thin layer of amplitude

transmittance t, that is expressed as

$$t(x, y; z) = \exp\left\{-\frac{1}{2}\alpha\left(|E(x, y; z)|^2\right)d + ik_0\Delta n\left(|E(x, y; z)|^2\right)d\right\},$$ (12)

where a constant phase factor has been ignored. The electrical field has absorbed a constant

factor so that we denote $I = |E|^2$. Taking Eq. (1) as the boundary condition, the effective

light field that will propagate through the layer of thickness d is given by

$$E_{eff}(x, y; z) = t(x, y; z)E(x, y; z).$$ (13)

This modified wavefront then propagates through the distance d as if it was a "uniform

linear medium" whose refractive index is constant. In other words, only diffraction effects

are considered for $E_{eff}(x, y; z)$.

A fast Fourier transform is used to convert the effective spatial light distribution,

$E_{eff}(x, y; z)$, into the angular plane-wave spectrum, $\Psi_{eff}(p, q; z)$, which satisfies

$$\Psi_{eff}(p, q; z) = \int_{-\infty}^{\infty}\int_{-\infty}^{\infty} E_{eff}(x, y; z)\exp[-i(px + qy)]dxdy$$

$$E_{eff}(p, q; z) = \int_{-\infty}^{\infty}\int_{-\infty}^{\infty}\Psi_{eff}(p, q; z)\exp[i(px + qy)]dpdq$$ (14)

The spectrum distribution is multiplied by the spatial transfer function of propagation of

distance d. The spatial transfer function of this paraxial propagation for this distance can be

expressed as

$$H(p, q; d) = \exp\left\{\frac{i(p^2 + q^2)d}{2k}\right\}$$

$$= \exp\left\{\frac{i\lambda_0 d(p^2 + q^2)}{4\pi n_0}\right\}$$ (15)

where p and q are coordinates for spatial angular frequencies and λ_0 is the free-space

9

wavelength of the incident beam. A followed inverse Fourier transform gives us the light distribution after the d-distance propagation. Thus

$$
\begin{aligned}
E(x, y; z+d) &= \mathrm{F}^{-1}\{H(p,q;d)\mathrm{F}\left[E_{eff}(x,y;z)\right]\} \\
&= \mathrm{F}^{-1}\{H(p,q;d)\mathrm{F}\left[t(x,y;z)E(x,y;z)\right]\},
\end{aligned}
\tag{16}
$$

where F and F^{-1} denote Fourier and inverse Fourier transforms, respectively. The near-field Fresnel diffraction is obtained by repeating the above process layer by layer to find out the wave evolution. The separated treatments have little effect on the accuracy of the field expression when d is small enough. This assumption is tested in the simulation by the fact that changing d in a certain range does not affect the final field distribution.

The focusing property of the beam in the medium is an important parameter. It determines the information storage density in that medium. We started with a waist size of 1 μm, a practical size for any meaningful optical storage. Because of the large divergent angle for this waist, we simulated a one-dimensional array in order to cope with the huge computing task without compromising the generality. For one-dimensional case, the complex amplitude of the electrical field, expressed by Eq. (1) can be replaced by

$$
E(x; z) = E_0 \sqrt{\frac{W_0}{W(z)}}\ \exp\left\{ikz - x^2\left(\frac{1}{W^2(z)} - \frac{ik}{2R(z)}\right) - i\frac{\phi(z)}{2}\right\},
\tag{17}
$$

the parameters are the same as defined in Eqs. (2)-(5). The propagation factor now has p as its sole variable. In the simulation, we use laser beam power, denoted by PWR, as a parameter. The one-dimensional Gaussian beam's intensity will be $I_0 = \frac{PWR}{W_0}\sqrt{\frac{2}{\pi}}$ while it

is $I_0 = \frac{2 \times PWR}{W_0^2\pi}$ for a two-dimensional case. A one-dimensional Gaussian beam is

generated and put into a 4096-point one-dimensional array. The BR film is assumed with a thickness of 600 μm. The film is divided into 300 thin layers. We assume that the waist size is focused onto a position 360 μm deep into the BR if no absorption and phase-change are present.

V. Computer simulations

Simulations were performed with two typical laser wavelengths. One is He-Ne's 632.8 nm, the other is Ar ion's 514.5 nm. They present different refractive index change properties. First, we consider the effect of the nonlinearity on the waist size of a Gaussian beam that propagates through a BR film. Besides determining the information density for bitwise storage, this is also useful for image hologram where a high density recording requires a small recording area onto the BR film. During this simulation, we choose the power of the laser beam to be 1.0, 0.1, 0.01 and 0.001 mW and keep the saturation intensity, I_s, unchanged. The incident waist position was focused 360 μm deep into the BR film provided there would be no nonlinearity presented. Because this is a one-dimensional simulation, we, when using intensity or power of the beam, assume that the size of the beam in the other dimension is 1 mm.

The relative change of beam waist size in BR as a function of the incident beam waist size at a variety of laser beam powers is shown in Figure 2. When the incident Gaussian beam is with a low power (0.01 mW and 0.001 mW), the actual waist size in BR
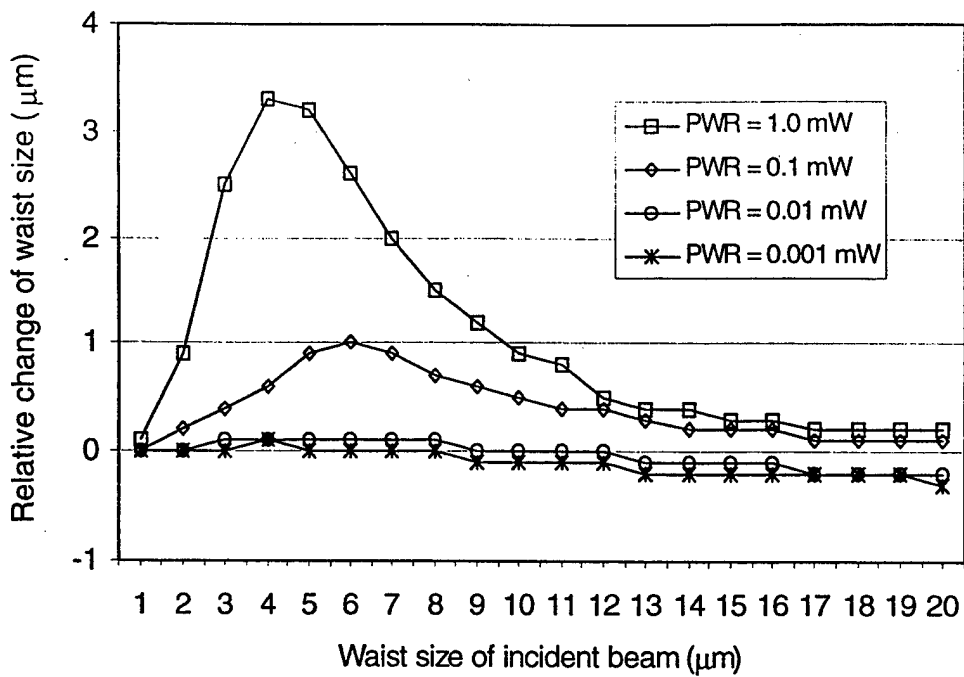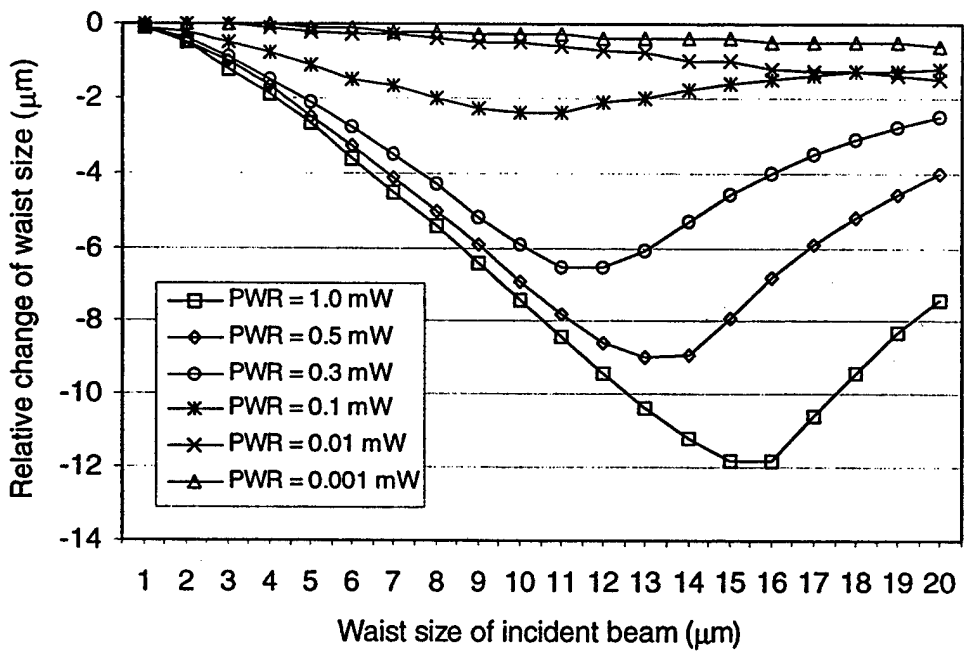
Figure 2. Influence of nonlinearity on the waist size of a Gaussian beam for (a) red light of 632.8 nm and (b) green light of 514.5 nm. The relative change is defined as the actual waist size minus the original incident waist size.

is almost the same as the incident beam size. The actual focused size is always smaller than that of the incident when the incident waist is large (i.e. incident waist size is about 10 μm or above). This is because the phase change effect is smaller than that of the amplitude absorption. The intensity-dependent absorption makes the waist size smaller because low intensity suffers a large absorption. When the beam power is high enough (0.1 mW and 1.0 mW), the actual waist differs greatly from the incident beam waist size. For a very small waist (1 or 2 μm) the intensity of the beam varies dramatically during its propagation because of its large divergent/convergent angle. Thus the major nonlinear effect affecting the waist size can only happen in a very limited space near the beam waist. Therefore the effect on the waist size change is small. But if waist size is large enough, the diverging angle is not large and thus the nonlinear effect can happen in a relatively long distance of beam propagation. The negative index change for He-Ne laser at a high intensity makes the converging beams divergent and reaches a waist phase distribution (i.e. uniform phase distribution) earlier than expected. Thus a larger-than-expected waist size yields. Even in the low incident waist regions of 0.01 mW or 0.001 mW this diverging effect is noticeable. The positive index change for 514.5 nm light enables the green light to be focused in a way opposite to that of the red light and forms a waist size much smaller than that of the incident wave. The most interesting results are with the power of 1.0 mW. As shown in Figure 2(b), the relative change of the waist size is almost proportional to the incident beam waist size. As the incident waist size increases, the actual waist size in BR does not increase that much and is kept around just a few microns. It is noted that when the incident waist size is larger than 16 μm, the actually-focused beam size increases as the incident waist size increases.
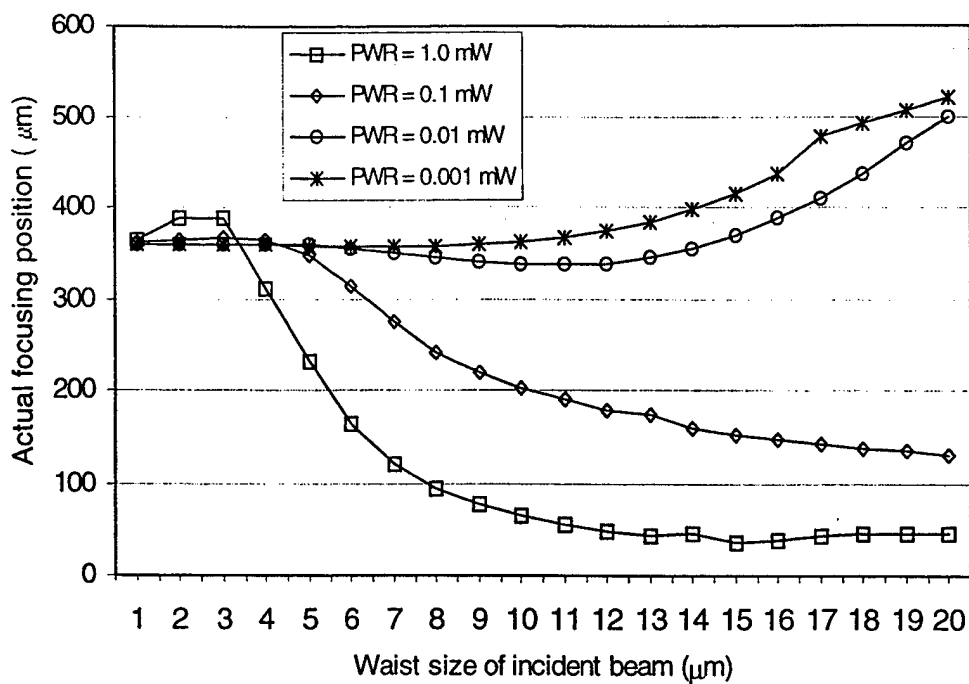
(a)
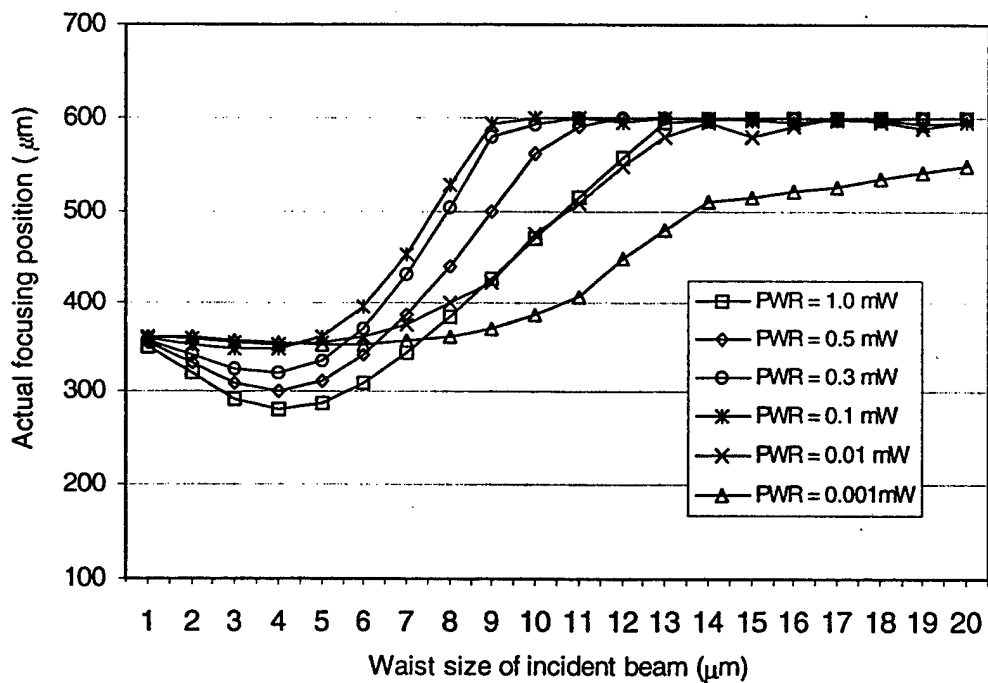
(b)

Figure 3.   Focusing position as a function of the incident beam's waist size for (a) red light of 632.8 nm and (b) green light of 514.5 nm. The incident light is supposed to be focused at 360 μm if no nonlinear absorption and phase modulation are present in BR.

This Phenomena is brought out because we only consider a film of 600 μm. The actual focus position is out of the film and our data just includes the minimum value inside film. This can be clearly seen with the help of Figure 3(b).

The relationship between the focusing position and the incident waist size was also simulated, as shown in Figure 3. As the plots show, the actual beam waist location in BR can differ greatly from that of the original incident beam, and the differences depend on the incident wavelength, incident waist size, and power. For the red light of 632.8-nm wavelength, the actual focusing position can be either ahead of or beyond the incident waist position. For a low beam power (0.01 mW and 0.001 mW), the beam intensity is low and the intensity-induced phase modulation slightly reduces the converging beam's convergence but not strongly enough to make the beam divergent quickly. Thus actual focusing position is moved a little bit towards the front surface of the BR film. Meanwhile the absorption modulation dominantly affects the focusing position. The weaker peripheral part of the Gaussian beam is strongly absorbed as the beam propagates and this effect always moves the position away behind the incident waist position. When the power is high, the diverging nature of strong index modulation makes the converging laser beam divergent before it can reach the incident waist position and yields a large actual focusing beam size. Exceptions are with the 1 to 3 μm region of the curve for 1.0 mW where the beam is with a large converging/diverging angle. Thus at the front surface of the BR film the beam size is large and the intensity is relatively low. The intensity distribution from the front surface to the focus point changes dramatically. First the intensity is low; thus the absorption takes a main role. Then the intensity becomes high, and the index change dominates the effect. The

15

above-mentioned exceptions are the combination with the absorption taking a main part. For the green light of 514.5 nm as shown in Figure 3(b), most of the focusing position for a large waist stops at 600 μm as the incident waist size increases. This is because we only consider a BR film that is 600-μm thick. The focused point have reached out the back surface of the BR film, hence the minimum beam size within the BR film is located at the back surface of the BR film. Where the curve reaches the 600-μm boundary corresponds to the turning point in Figure 2(b) of the corresponding curves. When the power is low (0.01 mW and 0.001 mW), absorption takes the main role influencing the focusing position. The curves are similar to what Figure 3(a) shows for the He-Ne low beam power. When the power increases (0.1 mW to 1.0 mW), the converging nature of the modulation makes the Gaussian beam a little more convergent and reaches focused position earlier than the incident waist position. The increase of incident beam waist size reduces the index phase modulation and strengthens the absorption modulation effect. Therefore the focusing position moves back to the back surface of the BR film. The results of Figures 2 and 3 indicate that the beam waist size and position will change in BR in a nonlinear manner and some of these changes are so big that they should be considered when memory position allocation is considered. In other words, pre-recording calibration is required in order to record reliable data in the BR film.

When we look at the incident waist position, that is, 360 μm, the actual beam sizes are different from that of the incident beam, as shown in Figure 4. The vertical axis denotes the actual beam width. For the He-Ne wavelength beam width is always larger than the incident waist size. The largest error occurs when the waist size is around 5 μm. The actual
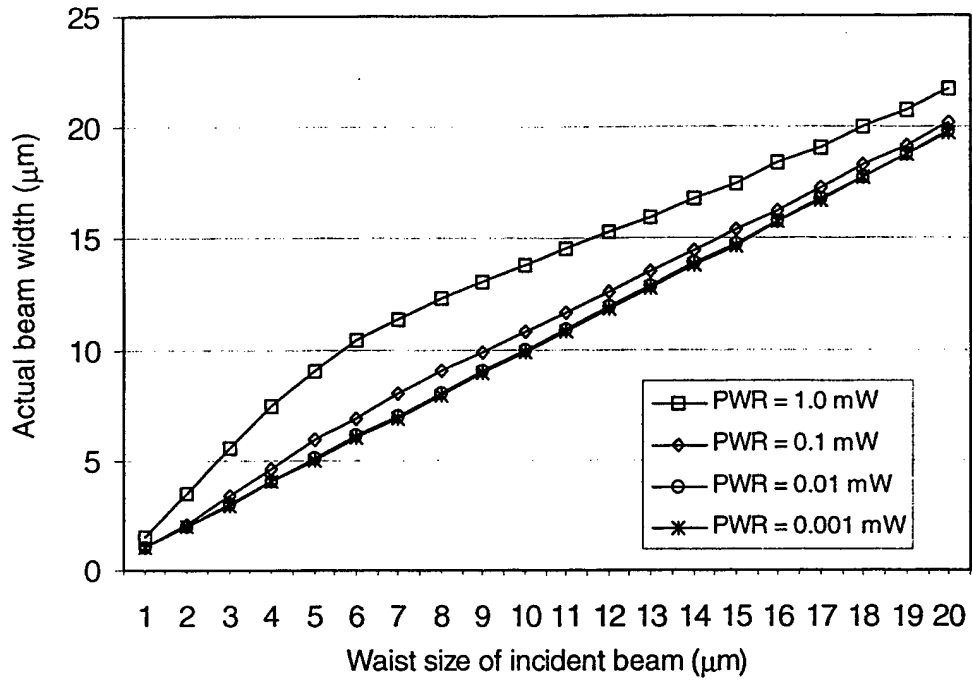
(a)
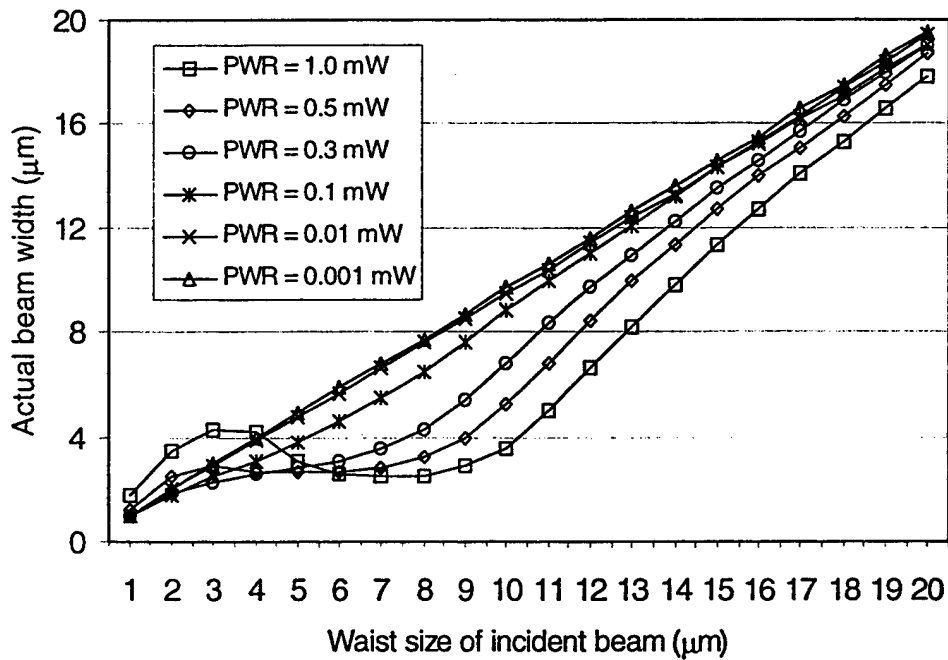
(b)

Figure 4.   Actual beam width at the original incident beam
waist position for (a) wavelength of 632.8 nm and (b)
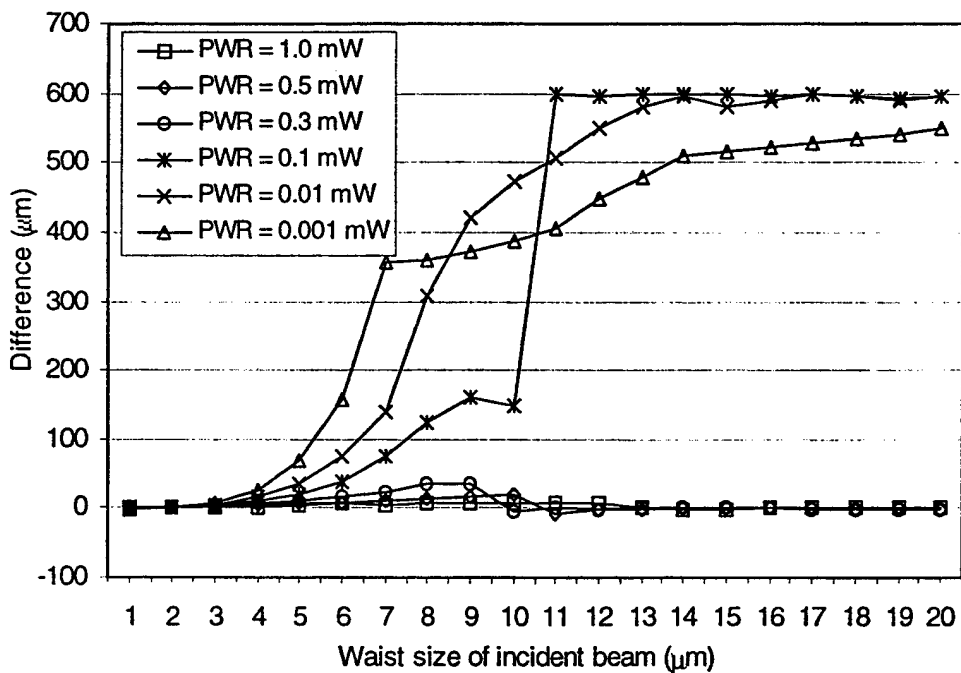wavelength of 514.5 nm.

beam width almost double that of the incident beam. But the case for an Ar green line is more complicated. In most of the case, the beam width at the expected focusing position has a reduced waist size. A larger-than-expected beam size occurs only when the expected waist size is small and beam power is high.

Because of the presence of both absorption and phase modulation in BR, the highest intensity does not occur at the position of the beam waist. The difference between these two positions as a function of incident waist size is depicted in Figure 5. Because this difference is caused by the absorption, the highest intensity generally occurs before the waist position. There is only one exception in the graph of the He-Ne light with the Gaussian beam power to be 1.0 mW and the target waist is 4 μm. The beam intensity profiles for this exception are drawn in Figure 6. Attention is given to three situations, the intensity distribution at the front surface of the BR, that at the focusing position and that at the maximum central intensity location. The first case is indicated by a thick line in the figure while the other two are represented by a medium line and a thin line, respectively. The first case is an ideal Gaussian distribution. But due to the nonlinear modulation, the beam intensity profiles for the second and third cases do not maintain a Gaussian shape, though very alike. When judged by the Gaussian waist size evaluation criteria, i.e. the distance between the locations where the intensity drops to $1/e^2$ of the central intensity, the second case is the best. There are also two exceptions for the green light at 10 μm and 11 μm. These are merely caused by simulation accuracy. When the beam power is high, as shown in Figure 5, the absorption effect does not take main part and the difference is not large. When the beam power becomes higher and higher, the difference gets larger and larger. There are turning points on
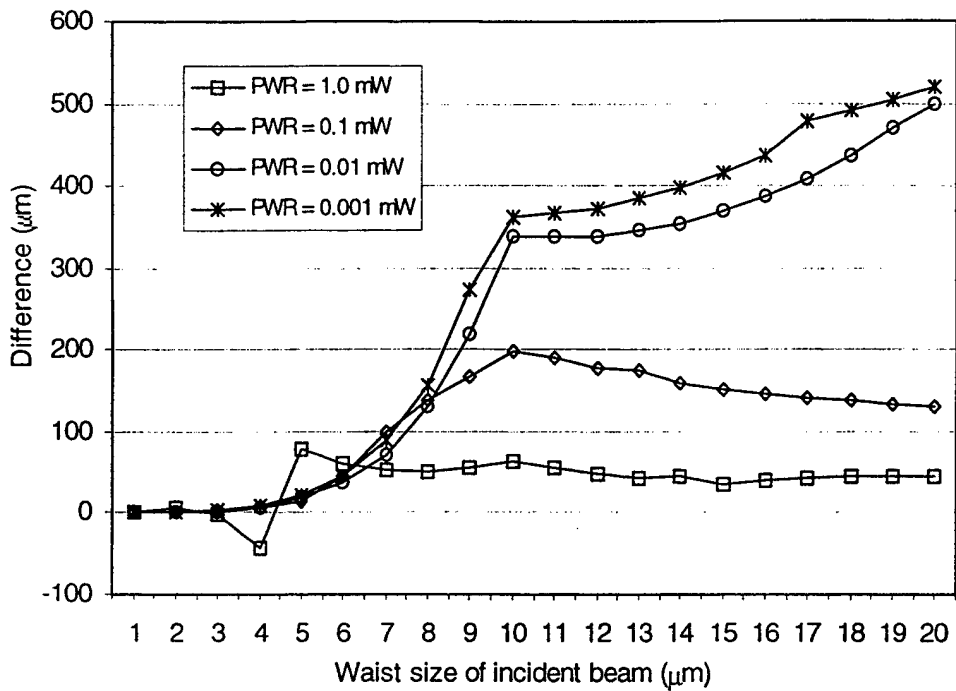
Figure 5. The difference between the beam waist position and the highest intensity position for (a) 632.8 nm wavelength and (b) 514.5 nm wavelength.
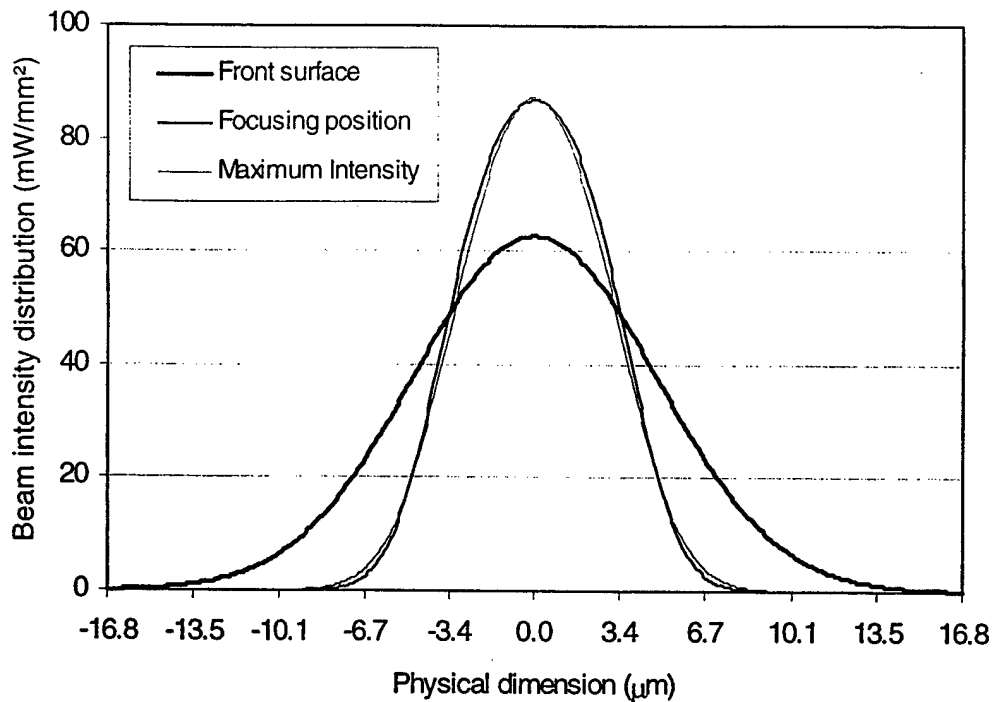
Figure 6.   Profiles of the beam's intensity distribution for the
red light at front surface of the BR film and positions inside the
BR film where we found the actual focus and maximum central
intensity. The incident beam power is 1.0 mW and the waist
size is 4 μm.

the low beam power curves. For the He-Ne light beam, turning points occur at a 10-μm

incident waist size with beam powers of 0.1 mW and 0.01 mW. That is when the

maximum-central-intensity point reaches the front surface. This position can not be moved

any further. Therefore further increase of the incident beam waist size see a slow increase of

the difference between the focusing position and the maximum central intensity position.

The situation is more complicated for green light. For the high beam powers (1.0 mW, 0.5

mW and 0.3 mW), there is little difference between the locations of focusing position and

maximum central intensity. As the incident beam waist increases, both these positions move

towards the back surface of the BR film. For the 0.1 mW beam power curve, the increase of

the incident waist size moves the maximum central intensity position towards the back

20

surface of the BR. But when incident waist is large than 11 μm, the absorption effect is so

strong that the central intensity at the front surface of the BR film is larger than any central

intensity in the film, and thus a huge jump is presented on this curve. To present this

situation clearly, Figure 7 shows the beam central intensity as a function of the BR film's

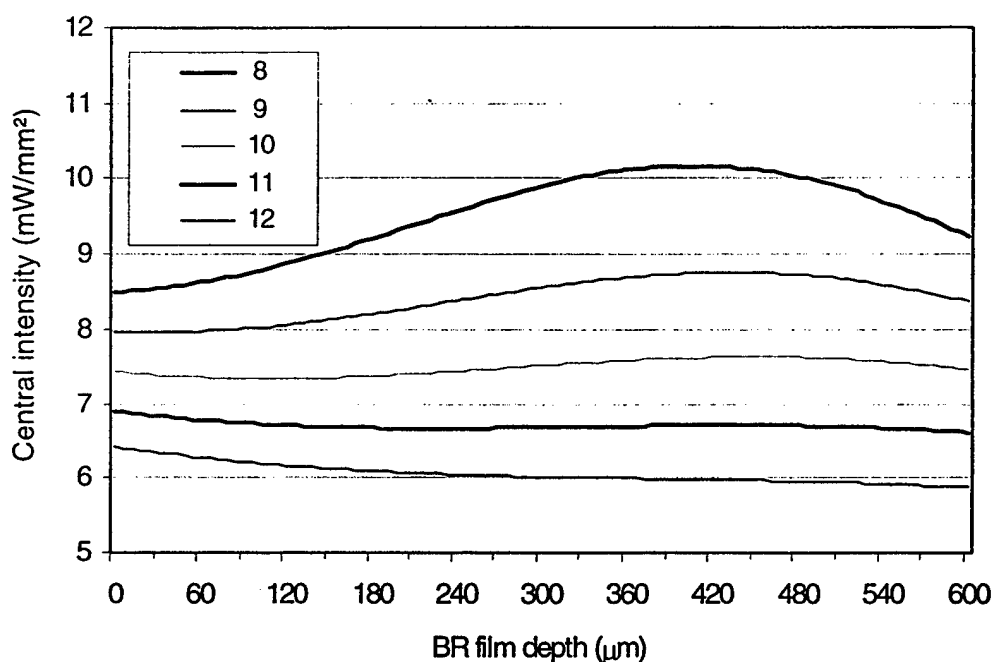depth for a number of incident waist sizes.

Figure 7.   Central intensity via BR film depth relationship for
a number of incident beam waist sizes at a beam power of 0.1
mW of green light. Curves from top to bottom are
corresponding to an incident waist size of 8, 9, 10, 11 and 12
μm.

The curves from top to bottom are corresponding to an incident waist size of 8, 9,

10, 11 and 12 μm. When incident waist size varies from 8 μm to 10 μm, the maximum

central intensity (peak value) moves towards the back surface of the BR film. When the

incident waist size becomes 11 μm, although the peak intensity moves in the same

direction, the maximum central intensity occurs at BR's front surface. The fact that the

21

maximum intensity no longer occurs at the beam waist is significant in 3-D optical memory

applications. In two-photon optical memory, the maximum intensity location is where the

two-photon absorption happens. In Fourier volume holographic memory, the location of the

maximum intensity should be considered for optimum interference modulation.

For the 632.8-nm wavelength the focused beam size is generally larger than the

incident beam waist while for the 514.5-nm wavelength the focused beam size can be

smaller than the waist size of the incident beam. This property for the green light may be

used to achieve a beam size smaller than the diffraction limit. We simulated the focused

beam size as a function of the illuminating beam power. The simulation results for an

incident waist position of 100 μm and 360 μm are shown in Figures 8 and 9, respectively.

Figure 8.   Waist size via the laser beam power for 632.8 nm
and 514.5 nm for incident waist sizes of 3, 5, 7 and 9 μm. The
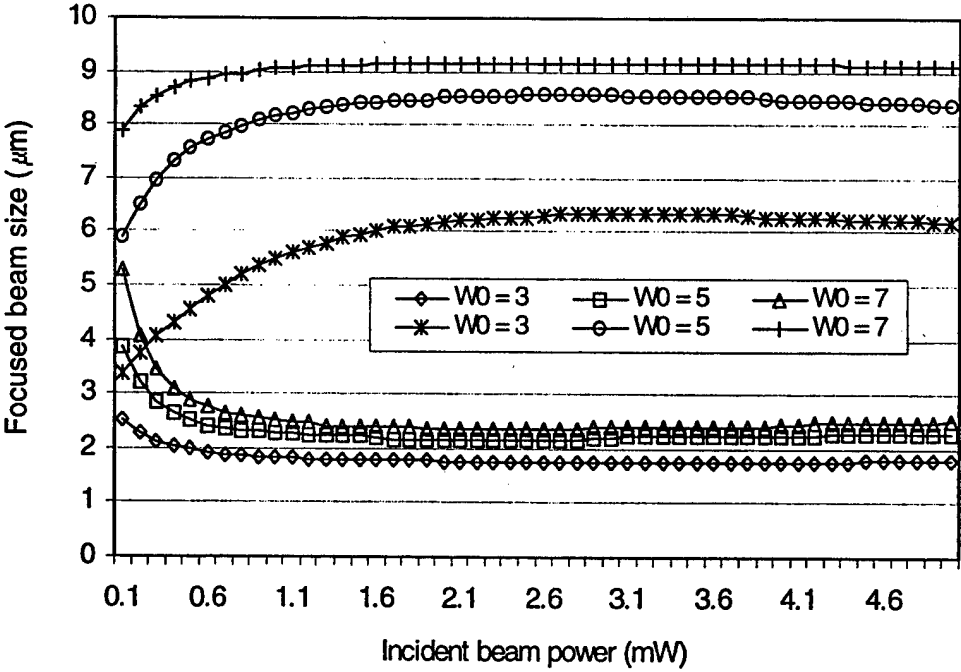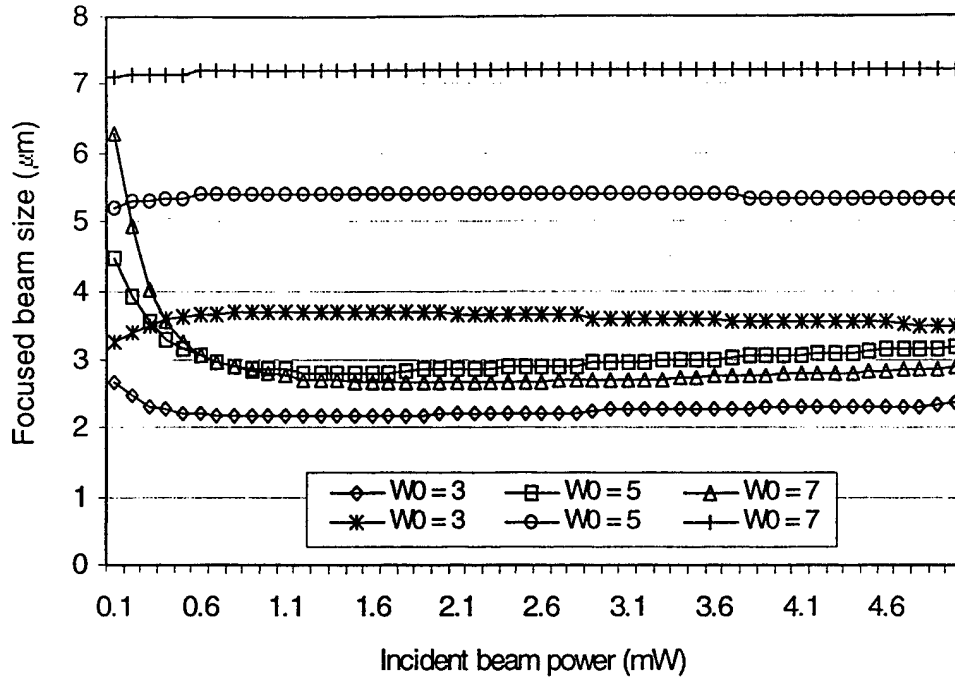incident waist position is 360 μm into the BR film.

Figure9.   Waist size via the laser beam power for 632.8 nm
and 514.5 nm for incident waist sizes of 3, 5, 7 and 9 μm. The
incident waist position is 100 μm into the BR film.

Both red and green wavelengths are considered with incident waist sizes of 3, 5 and

7 μm. The three top lines are for red light and the three bottom lines are for green light. For

both the green and red light, there exists a beam power at which an extremum focus size is

formed. The positive index change of the green light provides a converging lensing effect

and increases the converging angle of the Gaussian beam, hence a smaller beam size is

formed. The increase of the beam power intensifies the lensing effect and reduces the

focused beam size. For the red light there is a maximum focused size. As the beam power

increases from null, the increased index change makes the red to have larger and larger

focused size and the green light smaller and smaller one, as those curves shown in Figure 2.

But when the power is even higher, the saturation in absorption and index change expressed

by Eqs. (6) and (10) reduces the modulation on the incident beam and causes the red light's

23

focused size to decrease and the green light's focus size to increase. The beam power to reach an extremum waist size depends on the incident waist size and the incident focusing position. A small incident waist size requires a smaller beam power to result an extremum of focused beam size than that for a large incident waist size; and a short incident waist position, by comparing Figure 9 with Figure 8, can also provide the similar result.

VI. Conclusions

We have, with the 632.8-nm He-Ne laser wavelength and 514.5-nm Ar wavelength, numerically investigated the Gaussian beam propagation property through a thick BR film. It is shown that the focusing position and the waist size of the Gaussian beam are both affected by the nonlinearity of the BR material. Thus when using BR as the optical memory media these parameters should be taken into account in order to get an optimum and reliable recording. The method can also be applied to analyze other intensity-dependent absorption and phase modulation materials. From this simulation, it is also concluded that for a very large converging angle, i.e. an incident waist size under 1 μm, the focused beam size and position are not greatly influenced by the nonlinearity of the material.

References

1. S. Esener, J. E. Ford and S. Hunter, "Optical data storage and retrieval: research

directions for the 90's," Optical Technologies for Aerospace Sensing - Critical Reviews of Optical Science and Technology, J. E. Person, Ed., SPIE Volume **CR47**, 94-130 (1993).

2. B. Hesselink and M. Bashaw, "Optical memories implemented with photorefractive media," Opt. and Quantum Electronics, **25**, 611-661 (1993).

3. A. S. Dvornikov and P. M. Rentzepis, "2-photon 3-dimensional optical storage memory," Advances in Chem. **240**, 161-177 (1994).

4. R. R. Birge, "Nature of the primary photochemical events in rhodopsin and bacteriorhodopsin," Biochem. Biophys. Acta, **1016**, 293-327 (1990).

5. D. Desterhelt, C. Brauchle and N. Hampp, "Bacteriorhodopsin: a biological material for information processing," Quart. Rev. Biophys. **24**, 425-478 (1991).

6. Q. Wang Song, Chunping Zhang, Richard B. Gross, and Robert R. Birge, "The intensity-dependent refractive index of chemically enhanced bacteriorhodopsin," Optics Communications, **112**, 296-301 (1994).

7. Robert R. Birge, "Protein-based optical computing and memories," Computer, **25**, 56-67 (1992).

8. Robert R. Birge, "Protein-based three-dimensional memory," American Scientists, **82**, 348-355 (1994).

9. Q. Wang Song, Chunping Zhang, Richard Gross, and Robert Birge, "Optical limiting by chemically enhanced bacteriorhodopsin films," Optics Letters, **18**, 775-777 (1993).

10. Ofer Werner, Baruch Fischer, Aaron Lewis, and Isaiah Nebenzahl, "Saturation absorption, wave mixing, and phase conjugation with bacteriorhodopsin," Optics

Letters, **15**, 1117-1119 (1990).

11. Bahaa E. A. Saleh and Malvin Carl Teich, Fundamentals of Photonics, John Wiley & Sons, Inc., 1991.

12. Ofer Werner, Baruch Fischer, and Aaron Lewis, "Strong self-defocusing effect and four-wave mixing in bacteriorhodopsin," Optics Letters, **17**, 241-243 (1992).

13. Richard B. Gross, K. Can Izgi and Robert R. Birge, "Holographic thin films, spatial light modulators and optical associative memories based on bacteriorhodopsin," in *Image Storage and Retrieval Systems*, Proc. SPIE, **1662**, 186-196 (1992).

14. D. Zeisel and N. Hampp, "Spectral relationship of light-induce refractive index and absorption changes in bacteriorhodopsin films containing wildtype BR_{WT} and the variant BR_{D96N}, " J. Phys. Chem. **96**, 7788-7792 (1992).